Mass Spectrometry
DOI: 10.5702/massspectrometry.A0154

Original Article

Effect of the Surface Morphology of a Metal Film on Ion Yields in a Platinum-Film Surface-Assisted Laser Desorption/Ionization Mass Spectrometry

Kotaro Hashimoto[1], Kyosuke Kaneda[2], Taichi Shimazaki[1], Chouma Kurihashi[1], Shuhei Yamamoto[2], Riko Takata[1], Shota Nakanishi[2], and Issey Osaka[*,1]

[1]*Department of Pharmaceutical Engineering, Faculty of Engineering, Toyama Prefectural University, 5180 Kurokawa, Imizu-City, Toyama 939–0398, Japan*
[2]*KYOCERA Corporation, 6 Takedatobadonocho, Kyoto Fushimi-ku, Kyoto 612–8450, Japan*

Matrix-assisted laser desorption ionization (MALDI) and surface-assisted laser desorption ionization (SALDI) mass spectrometry (MS), which can detect biomolecules and polymers, are widely used in biochemistry and material science. Some compounds that are difficult to ionize using MALDI can be ionized using SALDI. However, it is difficult to obtain high ion yields using SALDI/MS. In this study, a fabricated platinum (Pt) film with nanostructures on the sample surface using a sputtering method was evaluated to determine the optimal metal film for ion yield in SALDI. The surface morphology of the Pt film was analyzed using scanning electron microscopy (SEM), atomic force microscopy (AFM), transmission electron microscopy (TEM), X-ray reflectivity (XRR), and ultraviolet–visible–near-infrared (UV-Vis-NIR) reflectance spectroscopy. The SEM, AFM, and TEM images of the Pt film showed the deposited metal film giving high ion yields of polyethylene glycol (PEG) in SALDI/MS with a Pt film (Pt-SALDI) that had a rough surface. The densities and reflectivity of films were analyzed by XRR and UV-Vis-NIR. The higher ion yields of PEG were obtained by Pt-SALDI with the Pt films with lower densities and reflectivity. This indicates that the deposition conditions for the Pt films significantly improved the ion yield in Pt-SALDI/MS. The Pt-SALDI has ionization capabilities different from those of MALDI. Therefore, optimization of Pt film for SALDI/MS and the MS imaging allows more compounds to be detected with higher sensitivity.

Please cite this article as: Mass Spectrom (Tokyo) 2024; 13(1): A0154

Keywords: MALDI, SALDI/MS, Pt film, morphology, ion yields

(Received August 8, 2024; Accepted September 21, 2024; advance publication released online October 29, 2024)

INTRODUCTION

Matrix-assisted laser desorption/ionization (MALDI) employs UV-absorbing low-molecular-weight organic compounds as matrices for facilitating ionization. The target molecules are desorbed and ionized by irradiating the matrix-sample co-crystals with a UV pulse laser.[1,2] The MALDI is a soft ionization technique that can ionize high molecular weight peptides and proteins without decomposition.[3,4] Furthermore, synthetic polymers and oligomers can be ionized by MALDI.[5,6] In MALDI mass spectrometry (MALDI/MS), a raster analysis can be performed by scanning the stage of the sample plate with each acquisition of the mass spectrum. MALDI/MS imaging has been reported as an application of raster analysis.[7,8] MALDI mass spectrometry imaging (MSI) has been used for the localization analysis of lipids and drugs in animal tissue sections.[9,10] Therefore, MALDI/MS, which combines MALDI with MS, is widely used in proteomics, metabolomics, and pharmaceutical and material sciences.

Achieving the homogeneous co-crystallization of the sample and matrix molecules, selecting an appropriate matrix, and using slices of animal tissue to suppress charge-up are necessary to obtain high-quality spectra using MALDI/MSI. Several sample preparation methods have been proposed for MALDI/MSI. Techniques such as automatic spraying devices for matrix solutions,[11–13] chemical vapor deposition (CVD),[14] and two-step deposition methods[15,16] have been developed for obtaining small and uniform crystals. These methods provide higher reproducibility than the traditional air-spray application methods used for matrix solutions. Furthermore, matrix selection is a crucial factor for achieving high sensitivity. The ion yield of the target molecules depends

*Correspondence to: Issey Osaka, *Department of Pharmaceutical Engineering, Faculty of Engineering, Toyama Prefectural University, 5180 Kurokawa, Imizu-City, Toyama 939–0398, Japan*, e-mail: o-issey@pu-toyama.ac.jp

on the physicochemical properties of both the sample and the matrix in MALDI. Matrices of polymers and biological materials have been reported.[17,18] The increase in the number of matrices for MALDI also increases the number of analytes that can be detected with high sensitivity using MALDI/MS. However, there is no universal matrix, and there are still compounds for which desorption ionization is difficult in MALDI. Surface-assisted laser desorption/ionization (SALDI) has been used to ionize such compounds.

In SALDI, reports have utilized UV-absorbing materials such as graphite,[19] metal nanoparticles,[20] and metal films[21–23] as ionization aids. Slicing the sample to suppress the charge-up is not essential for using conductive metal films as UV-absorbing materials in SALDI. This SALDI method simplifies sample preparation because it does not require optimization of the matrix-sample crystallization conditions required by MALDI. The MALDI/MS interprets the mass spectrum in the low-molecular-weight region attributed to the numerous peaks originating from the matrix. By contrast, SALDI can employ UV-absorbing materials that are not ionized.[20] In addition, SALDI, which has ionization capabilities different from those of MALDI, has been reported.[22] Therefore, SALDI can be used as a complementary method to MALDI.

Uniform metal films for SALDI can be obtained easily and automatically deposited on metal using sputtering[22] or mist CVD methods.[24] The metal films can be controlled at the nanometer level in both the X-Y plane and thickness. They are suitable for high-throughput analytical techniques such as SALDI/MSI.[25] Platinum (Pt) films fabricated by sputtering exhibit different ion yields in SALDI/MS depending on the deposition conditions: deposition time, sputtering power, pressure, and ambient gas. During sputtering, these conditions result in different surface morphologies of the obtained metal films. Thus, the morphology is related to the ion yield in SALDI. In this study, SALDI/MS was performed on Pt films fabricated under various conditions. The Pt films were analyzed using scanning electron microscopy (SEM), transmission electron microscopy (TEM), and atomic force microscopy (AFM) to evaluate the relationship between the ion yield and surface morphology. In addition, the density and reflectivity of the films were measured using X-ray reflectivity (XRR) and ultraviolet–visible–near-infrared (UV-Vis-NIR) reflectance spectroscopy to determine their physical properties.

EXPERIMENTAL

Materials

The silicon substrate was obtained from ASONE (Tokyo, Japan); reagent-grade acetone was purchased from WAKO Pure Chemical Industries (Osaka, Japan); and polyethylene glycol (PEG; Mw 600) was purchased from Tokyo Chemical Industry (Tokyo, Japan). A Pt disc (99.99% purity, diameter: 50 φ × 0.3 mm; Furuuchi Chemical Corporation, Tokyo, Japan) was used as the sputtering target.

Sample preparation

The ion yield in SALDI was evaluated using standard PEG applied uniformly to a sample plate. PEG was prepared in acetone at a concentration of 1.0 mg/mL. The PEG solution (5.0 mL) was dropped onto a Si substrate for spin coating, and the substrate was spun at 1000 rpm for 1 min using a spin coater (MS-A200, MIKASA, Tokyo, Japan). Then, the substrate was vacuum-dried in a desiccator to obtain a Si substrate uniformly coated with PEG. A Pt film was deposited on the sample substrate using a magnetron sputtering device (SVC-700RF I, SANYU ELECTRON, Tokyo, Japan) for Pt-SALDI/MS. The sputtering conditions were set at a sputtering power of 100 W and a distance of 10 cm between the metal target and the sample. The ambient gas in the sputtering system was either Ar or air, and the pressure was set to 1, 10, or 20 Pa. Sputtering was performed at deposition times of 5, 30, and 60 s. Pt films were fabricated under these conditions and evaluated. The experimental condition in sputtering is listed in Table 1.

Table 1. Summary of the different methods for Pt deposition.

Pt film	Gas	Pressure (Pa)	Deposition time (s)
1	Ar	1 Pa	5 s
2	Air		
3	Ar	10 Pa	
4	Air		
5	Ar	20 Pa	
6	Air		
7	Ar	1 Pa	30 s
8	Air		
9	Ar	10 Pa	
10	Air		
11	Ar	20 Pa	
12	Air		
13	Ar	1 Pa	60 s
14	Air		
15	Ar	10 Pa	
16	Air		
17	Ar	20 Pa	
18	Air		

Measurements

SALDI/MS is performed using the MALDI/MS instrument. A JMS-S3000 SpiralToFTM-plus time-of-flight mass spectrometer (JEOL, Tokyo, Japan) was used for the SALDI/MS measurements. The instrument was equipped with an Nd:YLF laser operated at 349 nm. The delay time was set as 100 ns. All measurements were performed in the positive ion and spiral modes. The laser intensity, detector voltage, and laser frequency were set as 60%, −1500 V, and 250 Hz, respectively. MS data analysis was performed using the software msTornado™ Analysis (JEOL, Tokyo, Japan). Each measurement was performed three times, and the average ion intensities were summarized. Each mass spectrum was obtained by accumulation of 100 laser shots, and each shot was performed at a different spot.

SEM was performed using a Hitachi High-Technologies S-4800 field-emission scanning electron microscope (Tokyo, Japan). The measurements were performed at an accelerated voltage of 10 kV. The TEM measurements were conducted using a Hitachi High-Technologies H-9500 transmission electron microscope (Tokyo, Japan). A Hitachi High-Technologies FB2100 (Tokyo, Japan) was used for the focused ion beam (FIB) measurements; the sample was thinned by processing stepwise decreasing accelerating voltages from 30 to 10 kV; the accelerating voltage was 200 kV. AFM measurements were performed using a Hitachi High-Technologies AFM5300E atomic force microscope

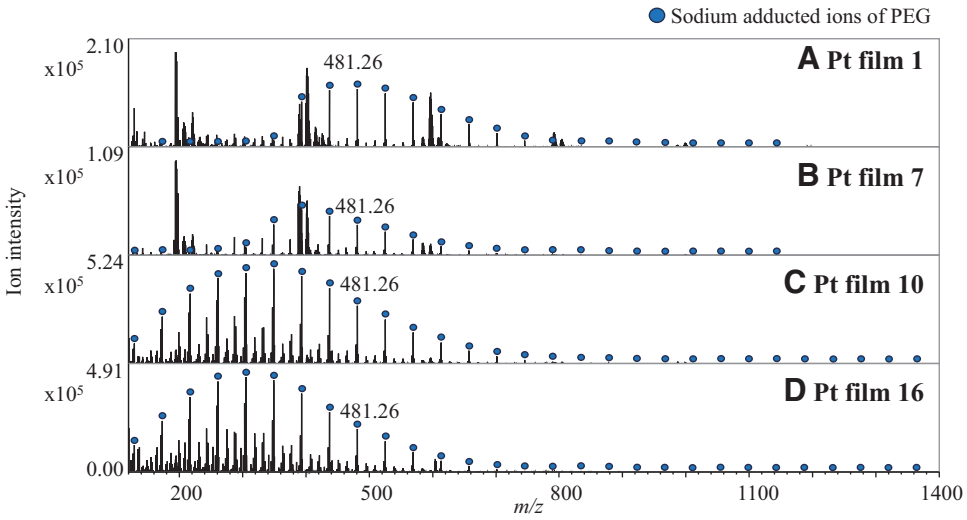

Fig. 1. Pt-SALDI mass spectra of PEG with each Pt film: (A) Pt film 1, (B) 7, (C) 10, and (D) 16. Pt-SALDI, Pt film surface-assisted laser desorption ionization.

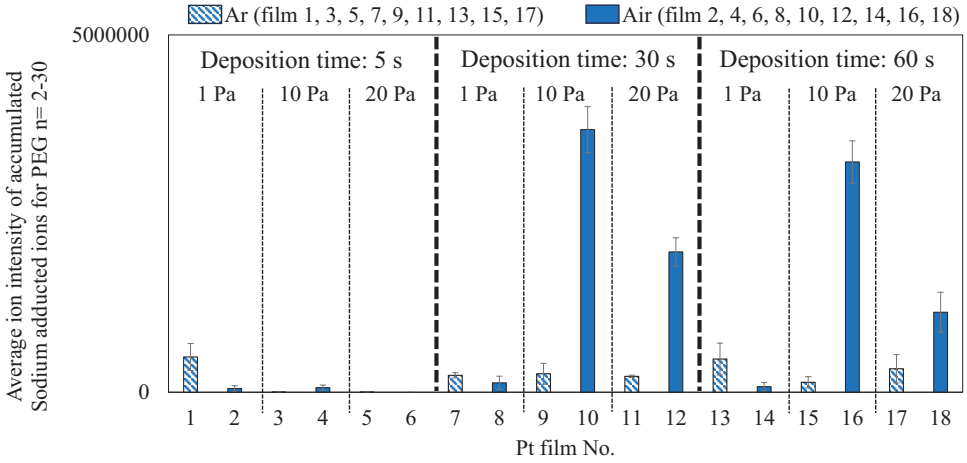

Fig. 2. Yields of PEG ions in Pt-SALDI/MS. Pt-SALDI/MS, Pt film surface-assisted laser desorption ionization/mass spectrometry; PEG, polyethylene glycol.

(Tokyo, Japan). A silicon probe (SI-DF40) was used for scanning in the DFM mode at a scanning speed of 0.5 Hz. The measurement area was a 500 nm square and evaluated at 512 × 256 pixels. The XRR measurements were performed using a PANalytical X'Pert PRO-MRD instrument (Almelo, Overijssel, The Netherlands). Cu-Kα radiation was used as the X-ray source with a generating voltage/current of 45 kV/40 mA, respectively. The measurement range was 0.1–6.0°, with measurements taken at 0.015° intervals and each step taking 5 s. UV-Vis-NIR spectrophotometry (Hitachi U-4100, Tokyo, Japan) was used for analyzing the Pt films deposited on the silicon substrates. The measurements were conducted in the wavelength range of 240–800 nm, evaluating the reflectivity at an incident light angle of 25° with a scan speed of 300 nm/min and a sampling interval of 1 nm.

RESULTS AND DISCUSSION

Ion yield of PEG obtained by SALDI/MS with a Pt film

The PEG was analyzed by SALDI/MS using Pt films prepared under deposition conditions 1–18. The mass spectra of Pt-SALDI/MS with Pt films 1, 7, 10, and 16 are shown in Fig. 1 and Supplementary Figure 1. In the spectra, sodium-adducted ions of PEG n = 2–30 were observed. The adducted sodium ions to PEG are contaminants from the environment. Detected m/z 481.26 is $[M_{n\ =\ 10}+Na]^+$ for the exact mass of 481.26. SALDI/MS with Pt film 10 affords high PEG ion yields. Each film was analyzed by Pt-SALDI three times. Ion intensities of sodium-adducted ions for PEG n = 2–30 were accumulated. The accumulated ion intensities were averaged and summarized in Fig. 2.

In the SALDI/MS experiments using Pt films 1–6 prepared at 1, 10, and 20 Pa with a deposition time of 5 s, the highest ion yields of PEG were obtained with Pt film 1. In the film prepared under air with a deposition time of 5 s, film 4 gave the highest ion yield. On the other hand, the ion yields were higher for deposition under air than under Ar at a deposition time of 30 s. At this deposition time, the highest ion yield was obtained with 10 Pa. P values from obtained ion intensities by Pt-SALDI/MS were calculated (Supplementary Table 1). The p values in film 10 and films 16, 12, and 18, giving high ion intensity, were 0.252 and 0.112, respectively. Both p values were more than 0.05. On the other hand, the p values in films

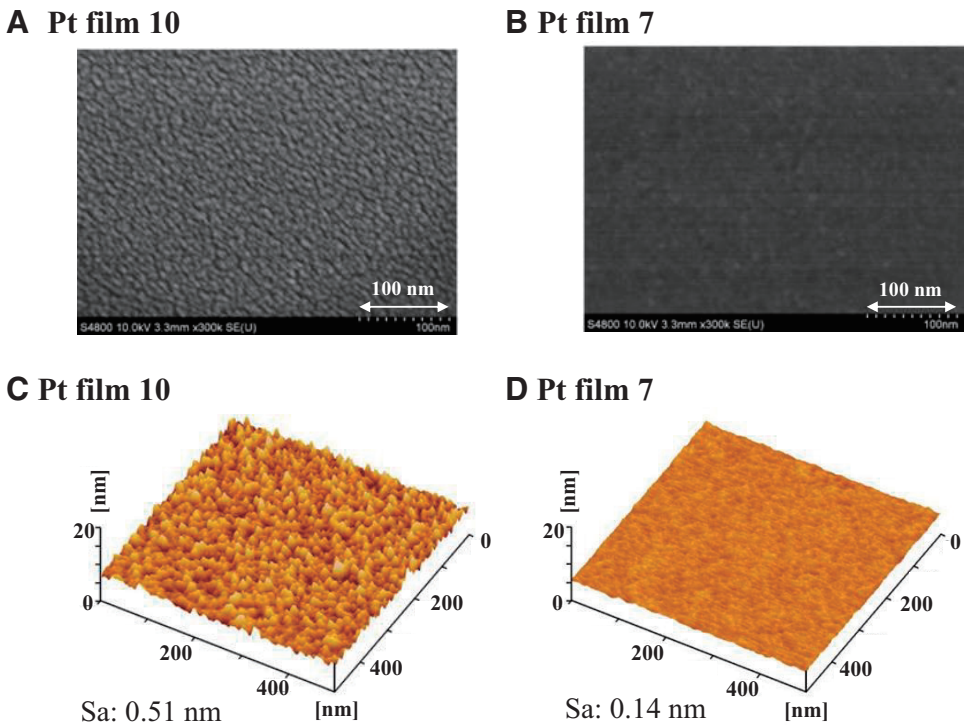

Fig. 3. SEM images of (A) Pt film 10 and (B) Pt film 7, and AFM images of (C) Pt film 10 and (D) Pt film 7. SEM, scanning electron microscopy.

4 and 10; 4 and 16; 6 and 12; and 6 and 18 were less than 0.05. Significant differences were identified in these *p* values. For sputtering in the air at 10 and 20 Pa, the Pt films obtained at a deposition time of 30 s and 60 s achieved significantly high ion yields. There was not enough Pt in the 5 s deposition under air and there was too much Pt in the 60 s deposition under air for SALDI. The ion yields were significantly different between 1 Pa and 20 Pa in the 30 s deposition. Films 13 and 17 had large RSD. In some cases of measurements, high ion yields of PEG could not be obtained. It is conceivable that the thick Pt film interfered with the passage of the produced ions for SALDI to the detector. The films 7, 9, 11, 13, 15, and 17 formed under Ar gave similarly low ion yields. The size of the obtained metal particles is highly dependent on pressure. The difference in the size of the metal particles has affected the ion yield.

The kinetic energy of the gas colliding with the metal must be controlled to obtain the target film structure during sputtering. The kinetic energy depends on the ionization potential, which is related to the energy of the incident ions and ionization fractions of the sputtered particles. The energy of the incident ions affects the sputtering rate. The sputtering rate of Pt under Ar is higher than that under air. At a constant pressure and deposition time, Pt films become thicker under Ar rather than in the air. Pt film 1 obtained under Ar for a deposition time of 5 s gave high ion yields due to the enough thickness. These results indicate that the surface roughness and thickness are important for thin films for SALDI.

The sputtered particles repeatedly collide with the gas, decreasing their kinetic energy and changing direction. The lower surface roughness of the metal film results in lower UV absorption by surface plasmon resonance and a lower ion yield in SALDI. The surface of a Pt thin film was analyzed to evaluate these relationships directly and in detail.

Evaluation of the Pt film morphology

Although Pt films 10 and 7 were formed with the same deposition time of 30 s, there was a significant difference in their film thicknesses and the ion yield of PEG obtained by Pt-SALDI/MS. Pt films 10 and 7 were analyzed using SEM to compare their surface morphologies. The SEM images are shown in Figs. 3A and 3B. The surface of Pt film 10 had nanostructures in which the metal particles were stacked. The black areas in the SEM images represent the pores. Ions generated by SALDI pass through these pores and are introduced into the MS. Pt film 7 had a lower roughness, the metal particles in the film were densely packed, and a uniform metal film with few pores was formed. The metal particles constituting the metal film of Pt film 7 are small, which results in smaller and fewer pores. The Pt film was formed on the sample, and therefore, it was difficult for the samples underneath the densely stacked film to be extracted into the gas phase during desorption ionization. Thus, there are significant differences in the ion yields of Pt films 10 and 7.

AFM was used to evaluate the surface roughness of the films. The results are presented in Figs. 3C and 3D. In the AFM image of Pt film 10, a rough surface was observed with an average surface roughness S_a of 0.51 nm. In the AFM image of Pt film 7, the Sa was 0.14 nm, which indicates a surface with no roughness. The surface roughness of Pt film 10 is approximately 10 times that of film 7. Pt film 10 contained pores, and localized surface plasmon resonance occurred at the prominent protrusion on the surface because of UV laser irradiation, which led to a higher ion yield in SALDI. A surface with fewer protrusions absorbed less UV light. It is

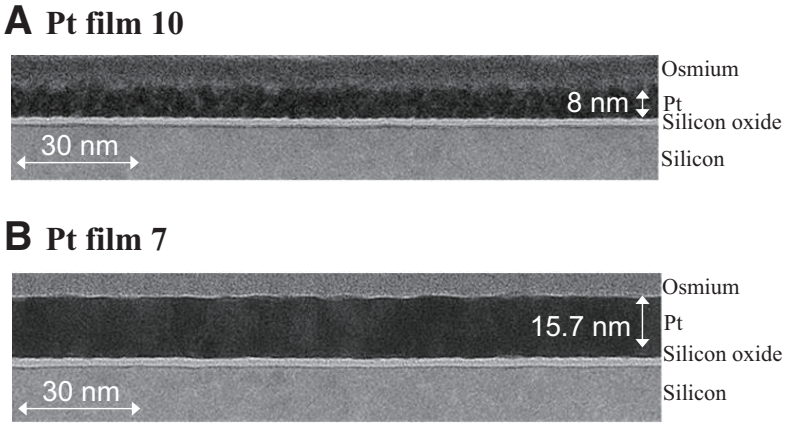

Fig. 4. TEM cross-section images of (A) Pt film10 and (B) Pt film 7. TEM, transmission electron microscopy.

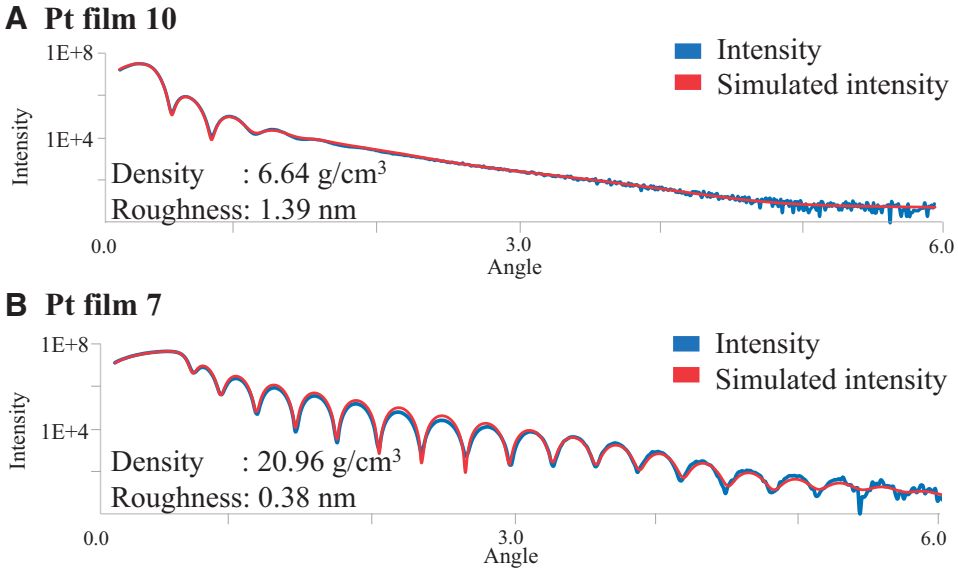

Fig. 5. XRR spectra of (A) Pt film 10 and (B) Pt film 7. XRR, X-ray reflectivity.

conceivable that the temperature of the deposited Pt was sufficiently lower than the melting point of Pt because there was a distance of 10 cm between the metal target and the sample substrate at a constant pressure in the system. Thornton[26] reported the effect of substrate temperature and gas pressure on the structure of metal films with high melting points in the zone model. The mean free path of the metal particles in the system becomes shorter when the gas pressure is high, and the movement direction of the metal particles changes because of scattering from the collisions with the gas particles. Therefore, the particles were incident on the sample substrate at an angle that affected the density of the film. The SEM and AFM results for Pt films 10 and 7 were consistent with those of the standard zone model.

Pt films 10 and 7 were also thinned using FIB, and the obtained cross-sections were observed by TEM. The TEM images are shown in Fig. 4. Each layer in the cross-section is from the top to the bottom: Osmium, Pt, silicon oxide, and silicon. Although the deposition times for Pt films 10 and 7 were the same, these images show significant differences in film thickness, which can be attributed to the mean free path for the deposition pressure and sputtering rate for the gas properties. In addition, large pores with grayish areas were observed in the Pt layer of the cross-section of Pt film 10. The film had a low density because a uniform film structure could not be formed. However, no pores were observed in Pt film 7.

The XRR analysis of the metal films was performed to evaluate the density. The corresponding spectra are shown in Fig. 5. Density and roughness were determined to fit the XRR data to the simulated curves. The densities of Pt film 10 and Pt film 7 were found to be 6.64 and 20.96 g/cm^3, respectively. The surface roughness of film 10 is approximately 3 times that of film 7, which is consistent with the TEM and AFM results. The surface roughness and density of the materials relate to their optical properties for surface plasmon resonance. The UV reflectivity of each film was analyzed; the results are presented in Fig. 6. The film with the highest ion yield in SALDI exhibited a substantial decrease in UV reflectivity. The decrease in reflection was attributed to the excitation of the surface plasmons. At the wavelength of 349 nm used by SALDI/MS, the reflectivity of Pt film 10 was ~50% of that of Pt film 7.

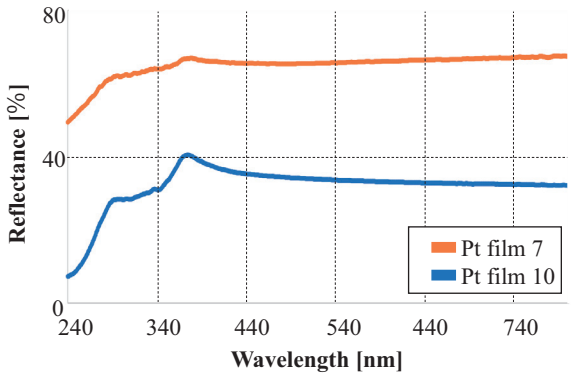

Fig. 6. UV-Vis-NIR diffuse reflectance spectra of Pt films 10 and 7. UV-Vis-NIR, ultraviolet–visible–near-infrared.

The ion yield of the PEG is higher in SALDI/MS with Pt films with lower densities and reflectivity. In addition, the rapid heating of nanoscale protrusions is crucial for SALDI. The surface properties of the films were important for SALDI. The results indicated that the optimal Pt film for SALDI/MS had a low density and rough surface with low UV reflectivity.

CONCLUSION

The Pt-SALDI/MS was performed using PEG samples prepared by spin coating. The relationship between the surface physical properties of the films and ion yield for SALDI was evaluated. The Pt films were analyzed by SEM, AFM, TEM, and XRR. Pt films with high surface roughness and low density exhibited high ion yields of PEG in Pt-SALDI/MS. The rough surface of Pt film has low UV reflectivity.

A Pt film with a rough surface, low density, and low reflectivity could potentially increase the ion yields of the target compounds in SALDI/MS. The optimized Pt film for SALDI/MS and the MS imaging allows more compounds to be detected with higher sensitivity.

ACKNOWLEDGMENTS

This work was supported by JSPS KAKENHI (grant number 23K11323) and Ame Hisaharu Foundation.

SUPPLEMENTARY INFORMATION

Supplementary Table 1. *P* values for *t*-test of PEG ion intensities by Pt-SALDI/MS.

Supplementary Figure 1. Pt-SALDI mass spectra of PEG with each Pt film: a) Pt film 2, b) 3, c) 4, d) 5, e) 6, f) 8, g) 9, h) 11, i) 12, j) 13, k) 14, l) 15, m) 17 and n) 18.

REFERENCES

1) M. Karas, F. Hillenkamp. Laser desorption ionization of proteins with molecular masses exceeding 10,000 daltons. *Anal. Chem*. 60: 2299–2301, 1988.
2) K. Tanaka, H. Waki, Y. Ido, S. Akita, Y. Yoshida, T. Yoshida, T. Matsuo. Protein and polymer analyses up to *m/z* 100 000 by laser ionization time-of-flight mass spectrometry. *Rapid Commun. Mass Spectrom*. 2: 151–153, 1988.
3) R. Aebersold, D. R. Goodlett. Mass spectrometry in proteomics. *Chem. Rev.* 101: 269–295, 2001.
4) M. Mann, G. Talbo. Developments in matrix-assisted laser desorption/ionization peptide mass spectrometry. *Curr. Opin. Biotechnol.* 7: 11–19, 1996.
5) L. Li. *MALDI Mass Spectrometry for Synthetic Polymer Analysis*, Wiley, 2010.
6) G. Montaudo, F. Samperi, M. S. Montaudo. Characterization of synthetic polymers by MALDI-MS. *Prog. Polym. Sci*. 31: 277–357, 2006.
7) M. Stoeckli, T. B. Farmer, R. M. Caprioli. Automated mass spectrometry imaging with a matrix-assisted laser desorption ionization time-of-flight instrument. *J. Am. Soc. Mass Spectrom*. 10: 67–71, 1999.
8) R. W. Garden, J. V. Sweedler. Heterogeneity within MALDI samples as revealed by mass spectrometric imaging. *Anal. Chem*. 72: 30–36, 2000.
9) K. A. Zemski Berry, J. A. Hankin, R. M. Barkley, J. M. Spraggins, R. M. Caprioli, R. C. Murphy. MALDI imaging of lipid biochemistry in tissues by mass spectrometry. *Chem. Rev*. 111: 6491–6512, 2011.
10) S. R. Shanta, T. Y. Kim, J. H. Hong, J. H. Lee, C. Y. Shin, K.-H. Kim, Y. H. Kim, S. K. Kim, K. P. Kim. A new combination MALDImatrix for small molecule analysis: Application to imaging mass spectrometry for drugs and metabolites. *Analyst* 137: 5757–5762, 2012.
11) M. Schuerenberg, S.-O. Deininger. Matrix application with ImagePrep. in Imaging Mass Spectrometry: Protocols for Mass Microscopy (Ed: M. Setou), Springer, Tokyo, 2010, pp. 87–91.
12) L. Meng, J. Han, J. Chen, X. Wang, X. Huang, H. Liu, Z. Nie. Development of an automatic ultrasonic matrix sprayer for matrix-assisted laser desorption/ionization mass spectrometry imaging. *Anal. Chem*. 94: 6457–6462, 2022.
13) C. R. Anderton, R. K. Chu, N. Tolić, A. Creissen, L. Paša-Tolić. Utilizing a robotic sprayer for high lateral and mass resolution MALDI FT-ICR MSI of microbial cultures. *J. Am. Soc. Mass Spectrom*. 27: 556–559, 2016.
14) J. A. Hankin, R. M. Barkley, R. C. Murphy. Sublimation as a method of matrix application for mass spectrometric imaging. *J. Am. Soc. Mass Spectrom*. 18: 1646–1652, 2007.
15) W. Bouschen, O. Schulz, D. Eikel, B. Spengler. Matrix vapor deposition/recrystallization and dedicated spray preparation for high-resolution scanning microprobe matrix-assisted laser desorption/ionization imaging mass spectrometry (SMALDI-MS) of tissue and single cells. *Rapid Commun. Mass Spectrom*. 24: 355–364, 2010.
16) S. Shimma, Y. Takashima, J. Hashimoto, K. Yonemori, K. Tamura, A. Hamada. Alternative two-step matrix application method for imaging mass spectrometry to avoid tissue shrinkage and improve ionization efficiency. *J. Mass Spectrom*. 48: 1285–1290, 2013.
17) M. W. F. Nielen. MALDI time-of-flight mass spectrometry of synthetic polymers. *Mass Spectrom. Rev.* 18: 309–344, 1999.
18) L. Charles. MALDI of synthetic polymers with labile end-groups. *Mass Spectrom. Rev.* 33: 523–543, 2014.
19) J. Sunner, E. Dratz, Y.-C. Chen. Graphite surface-assisted laser desorption/ionization time-of-flight mass spectrometry of peptides and proteins from liquid solutions. *Anal. Chem*. 67: 4335–4342, 1995.
20) R. Arakawa, H. Kawasaki. Functionalized nanoparticles and nanostructured surfaces for surface-assisted laser desorption/ionization mass spectrometry. *Anal. Sci*. 26: 1229–1240, 2010.
21) T. Ozawa, I. Osaka, S. Hamada, T. Murakami, A. Miyazato, H. Kawasaki, R. Arakawa. Direct imaging mass spectrometry of plant leaves using surface-assisted laser desorption/ionization with sputter-deposited platinum film. *Anal. Sci*. 32: 587–591, 2016.
22) T. Ozawa, I. Osaka, T. Ihozaki, S. Hamada, Y. Kuroda, T. Murakami, A. Miyazato, H. Kawasaki, R. Arakawa. Simultaneous detection of phosphatidylcholines and glycerolipids using matrix-enhanced surface-assisted laser desorption/ionization-mass spectrometry with sputter-deposited platinum film. *J. Mass Spectrom*. 50: 1264–1269, 2015.

23) K. Nozaki, Y. Nakabayashi, T. Murakami, A. Miyazato, I. Osaka. Novel approach to enhance sensitivity in surface-assisted laser desorption/ionization mass spectrometry imaging using deposited organic-inorganic hybrid matrices. *J. Mass Spectrom.* 54: 612–619, 2019.
24) R. Takata, Y. Nakabayashi, K. Hashimoto, A. Miyazato, I. Osaka. Imaging analysis of phosphatidylcholines and diacylglycerols using surface-assisted laser desorption/ionization mass spectrometry with metal film formed by mist chemical vapor deposition. *Mass Spectrom. (Tokyo)* 12: A0135, 2023.
25) W. H. Müller, A. Verdin, E. De Pauw, C. Malherbe, G. Eppe. Surface-assisted laser desorption/ionization mass spectrometry imaging: A review. *Mass Spectrom. Rev.* 41: 373–420, 2022.
26) J. A. Thornton. High rate thick film growth. *Annu. Rev. Mater. Sci.* 7: 239–260, 1977.